THÜNEN

Institute of Baltic Sea Fisheries (OF)

Alter Hafen Süd 2, 18069 Rostock Fon +49 381 66099-122 Fax +49 381 8116-199 Date 30.08.2024 E-Mail: juan.santos@thuenen.de

Cruise Report
FRV „Solea" Cruise 828
27.10 – 03.11.2023

Scientists in charge
Mathis Mahler (RT1)
Juan Santos (Cruise leader, RT2)

Übersicht

Die FFS-Reise "Solea" Nr. 828 war zwei Forschungsthemen gewidmet. Das erste Thema war der erstmalige Einsatz eines neuen Unterwasser-kamerasystems bei Fangversuchen. Diese Kamera wurde vom OTC-SmartFishing Konsortium entwickelt. Das Kamerakonzept zielt darauf ab, Echtzeitbeobachtungen innerhalb des Schleppnetzes zu ermöglichen und seine visuellen Fähigkeiten mit KI-basierten Technologien zu kombinieren, um Fische während des Fischens zu erkennen und zu verfolgen. Die während dieser Reise gesammelten Daten werden dazu beitragen, die Kameratechnologie weiterzuentwickeln und die für die Unterwasser-Fischdetektion entwickelten KI-Tools zu trainieren. Das zweite Forschungsthema ist ein Beitrag zum Verständnis des Fluchtverhaltens von Plattfischen in Schleppnetzen. Aktuelle Videobeobachtungen haben gezeigt, dass das Verhalten der Fische während des Selektionsprozesses einen erheblichen Einfluss auf das endgültige Schicksal der Fische hat. Dieses Verhalten, insbesondere die Orientierung der Plattfische zum Netz (idealerweise Körpertiefe parallel zur größeren Maschenöffnung), kann den Fluchterfolg beeinflussen. Das Verständnis und die Quantifizierung der Rolle des Verhaltens von Plattfischen bei Fluchtversuchen durch die Maschen kann die Entwicklung zukünftiger Schleppnetze mit präziserer Größenselektion für diese und andere Arten unterstützen. Diese Forschung ist von großer Bedeutung für die Ostseefischerei und alle anderen Schleppnetzfischereien, in denen Plattfische wichtige Ziel- oder Beifangarten sind. Die Reise fand ganz in den Fischereigründen bei Warnemünde (südwestliche Ostsee, ICES SD 22-24) statt.

Distribution list:

schiffsführung FFS „Solea" „Walther Herwig III" „Clupea"
BA für Landwirtschaft und Ernährung (BLE) Fischereiforschung
BM für Ernährung und Landwirtschaft (BMEL), Ref. 614
BA für Seeschifffahrt und Hydrographie (BSH), Hamburg
Deutscher Angelfischerverband e.V.
Deutsche Fischfang-Union, Cuxhaven
Deutscher Fischereiverband Hamburg
Doggerbank Seefischerei GmbH, Bremerhaven
Erzeugergemeinschaft der Deutschen Krabbenfischer GmbH
Euro-Baltic Mukran
Kutter- und Küstenfisch Sassnitz
LA für Landwirtschaft, Lebensmittels. und Fischerei (LALLF)
LA für Landwirtschaft und Fischerei MV (LFA)
Leibniz-Institut für Ostseeforschung Warnemünde
GEOMAR Helmholtz-Zentrum für Ozeanforschung Kiel
Thünen-Institute - Institute of Fisheries Ecology
Thünen-Institute - Institute of Sea Fisheries
Thünen-Institute – Institute of Baltic Sea Fisheries
Thünen-Institute – Press office, Dr. Welling
Thünen-Institute – Presidential office
Thünen-Institute – Scheduling research vessels, Dr. Rohlf
Fahrtteilnehmer*innen

1 Introduction to Research Topics (RT)

Research Topic 1 (RT1):

Up until recently the catch of a trawl is a black box that is mostly unknown, only when it is brought on deck the catch can be identified. This has changed with the development of underwater cameras and the ability to establish a constant video connection to the trawl. OTC-SmartFishing aims to use these technological developments and take it one step further. Not only do we want to observe the happenings in the trawl, but plan on detecting fish while trawling, in order to get information of the fish populations entering the trawl. For that purpose, a stereo-camera-system was developed and an artificial neural network (AI) was trained to detect fish in the video images. This system could, in it's final stage, supplement or even replace quantitative methods based on catch-data that are currently applied in fisheries research, because most of the relevant information (species and sizes) could be obtained accurately by the camera system. Sea trials conducted during the present cruise continue with our development work of these new tools. The aim was to test the camera-system now for the first time in fishing trials. The collection of data made on this cruise will help in further developing the camera technologies and the training of the AI tools devoted for underwater fish recognition.

Research Topic 2 (RT2): A contribution to the understanding of flatfish escape behavior in trawl codends: the relevance of mesh position relative to body orientation

Size selection in trawl gears can be defined as the ability of a fish to pass through the codend meshes. It is generally assumed that such ability is largely determined by the morphology and the size of the fish, and the geometry and the size of the mesh through which the individual is attempting to escape. In recent years, the availability of low-cost, compact cameras delivering high quality footage has facilitated the collection of direct observations of size selection in the codend. These observations show that the behavior of the fish accumulated in the codend can be a relevant factor to consider in order to better understand the mechanisms involved in the size selection. However, this information is not included in the traditional methods used to quantify codend size selection based on catch data analysis. Therefore, understanding the behaviour of fish species attempting to escape through the codend may open new avenues for the development of the next generation of trawl codends, characterized by well-defined and precise size selection.

There are a number of proof-of-concept studies suggesting that diamond-mesh codends provide better escape possibilities to flatfish species than other mesh geometries (for example square-mesh and T90 codends). This is because the flat morphology of these species can fit better to the diamond geometry adopted by the mesh openings under the towing forces. However, due to the distinct laterally compressed body morphology of flatfish species, it is reasonable to assume that the benefits associated with attempting to escape through a diamond mesh will only be available if the flatfish makes optimum contact with it. Here, we define optimal contact when the transversal

axis of the fish (body depth) is parallel to the wider axis of the mesh opening. Positioning the body in a way that ensures an optimum contact can be energetically demanding depending on how the fish is positioned relative to the mesh. In general, it has been shown that fish often engage in energetically efficient behaviors during the capture process. Therefore, in the context of size selection, It can be hypothesized that escape opportunities that require simple body rotation and limited hydrodynamic disturbance to use will be preferred over other more demanding escape paths available. A graphical explanation of this argumentation can be found in Figure 1.

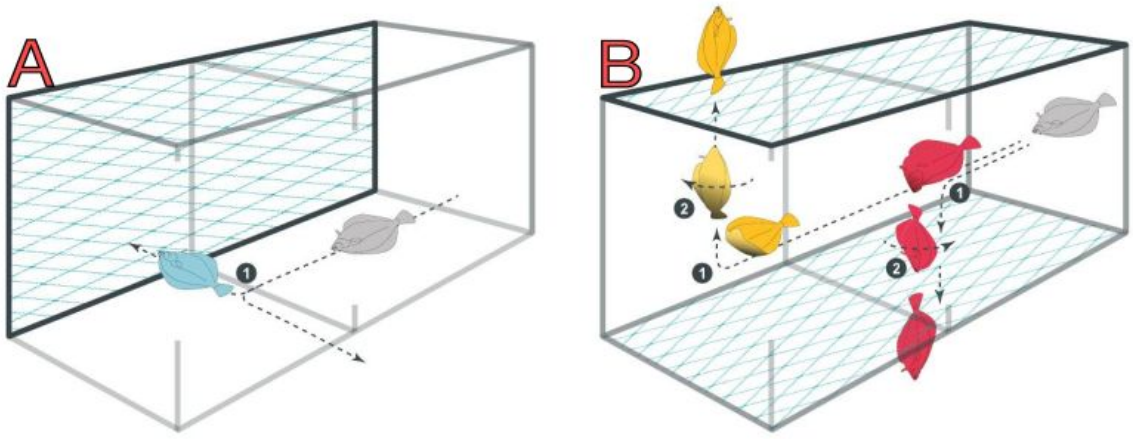

Figure 1: Flatfish in a cuboid structure covered with diamond mesh and theoretical escape pathways. The gray flatfish shape assumes the same initial body position in both scenarios. To achieve optimum contact with the mesh openings, the escape path shown in Scenario A requires only one turn of the fish's body. The path towards optimal contact with the mesh showed in scenario B is more complex as it requires two body turns, the first of which positions the broad axis of the flatfish body perpendicular to the expected flow of water during towing. It can be therefore assumed that escapes attempt represented in scenario A will be more energetically efficient than those represented in Scenario B.

Experimentally testing the hypothesis outlined above can add new and valuable knowledge regarding how flatfish is size-selected in codend gears. Therefore, part of the present cruise will be devoted to sea trials associated to this RT2. By running and innovative experiment specifically designed for such a purpose, we aim to improve the understanding of flatfish escape behavior in trawl codends.

2 Material and Methods

The two research topics were addressed one after the other along the seven fishing days available of the cruise. Fishing activities related to live camera technologies development (RT1) were carried out in the first three days of the cruise (27.10.2023 - 29.10.23), and the remaining fishing days available (30.10.2023 - 02.11.2023) were allocated to RT2. Sea trials took place entirely at fishing grounds of Warnemünde / Nienhagen (statistical ICES rectangle 37G2). Fishing activities associated to both RT's were conducted using a trawl model TV300/60 spread by two doors Thyboron Type 2 (1.78 m²) and 50 m sweeps. Specific details of the materials and methods related to each RT are provided separately below.

2.1 Research Topic 1

During the first 2 fishing days of the cruise experiments were conducted to test the newly developed SmartFishing-Camerasystem. The system was installed in the NEMOS-tunnel (Figure 2), in front of the codend. The System consists of a Stereo-Camera, two adjacent LED-Lights, a Controller-unit and a Battery-unit.

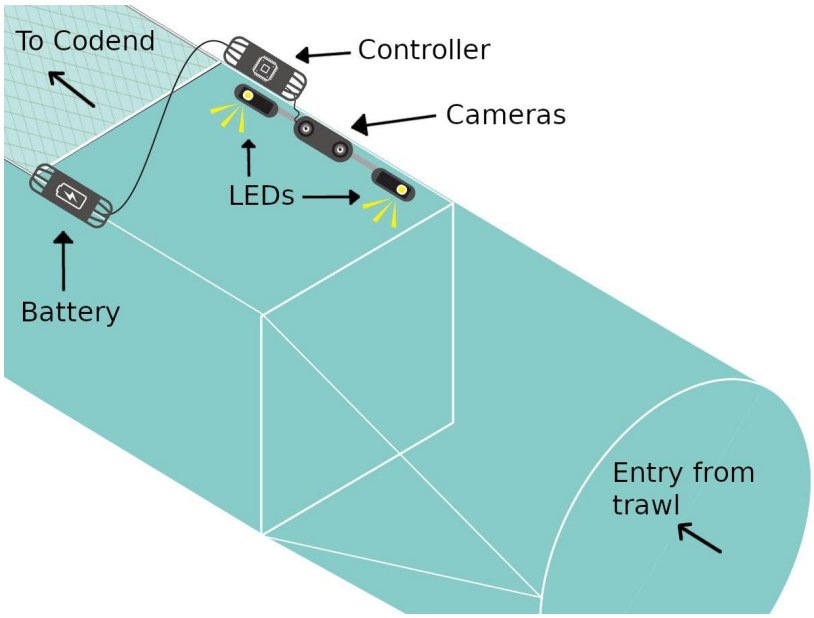

Figure 2: Schematic setup of SmartFishing-System in NEMOS-tunnel.

The structure of Cameras and Lights on a POM-rod were fixed to the corners of the tunnel with cable straps, the Controller and Battery were fixed with snap hooks as seen in (Figure 3). The structure of the tunnel was supported by floats, as can be seen in (Figure 4). The Structure was stable, but the Floats on top of the net-opening (white Rhombus) where lifting too much and should be reduced in future trials.

Figure 3: SmartFishing-System in NEMOS-tunnel.

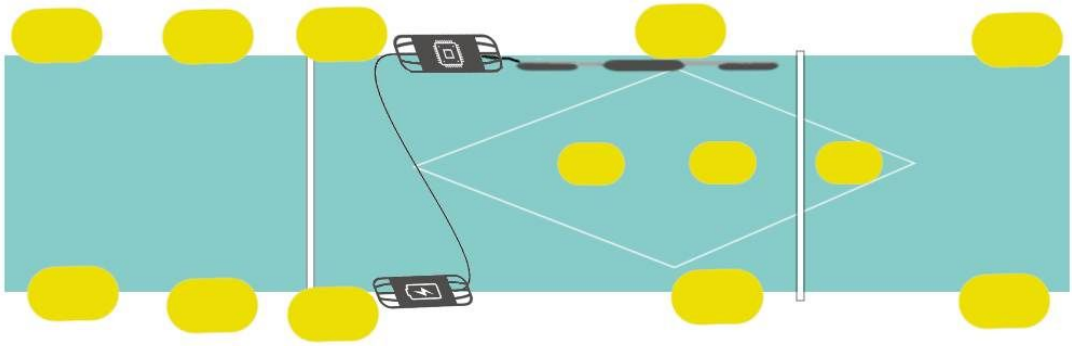

Figure 4: Floats Setup NEMOS tunnel with SmartFishing-System (small yellow floats symbolize 2kg, bigger ones are 5 kg).

The connecting cable to the vessel (orange cable coming from the top in Figure 2) is being fixed to the trawl with snap hooks while deploying it. They are taken off, while recovering the net, in order to avoid the cable to be damaged on the drum of the winch. Also the Camera-System itself should not be rolled up on the winch yet, because, in it current state, it is likely to take damage.

The connection will turn over to a stronger dyneema-cable, that is being managed by a winch from LFish, specially customised by Framework Robotics, at deck. For mounting the winch on FS Solea, the foundation of a MacArtney-Winch was used. The used winch has an automatic loosening and tightening control, therefor the winch does not need an operator during the whole haul, only when deploying and retrieving the net. The winch is depicted in Figure 5.

Figure 5: LFish-Winch on Solea.

During fishing the haul images from the SmartFishing-System could be observed at a Laptop on the vessel.

2.2 Research Topic 2

Only the last four days of the cruise (between 30 October and 2 November 2023) were available to carry out this experiment. Due to this limited number of fishing days, each codend design was tested for one day during five consecutive and valid hauls. To reduce sources of uncontrolled variation, fishing activities were conducted on the same fishing grounds, fishing depths and daytime. The experiment was conducted using the cover-codend method, enabling direct observation of the retained and escaped fish at haul level.

Experimental codend designs

The experimental designed to address RT2 involved the quantification of the selectivity of four different codend setups (Figure 6). These designs are modifications from a rigid codend with a mesh size of ~110 mm and a diamond-mesh geometry fixed to an Opening Angle (OA) ~ 40° (Fixed Diamond 40°, FD40_110) This codend was already used in the 2021 FRV “Solea” cruise no 797

(here the link to the cruise report). The three remaining designs were achieved by "blinding" one or more sides of the FD40_110 codend. This was done by using small-mesh inlet panels. The nominal mesh size (Fonteyne *et al.*, 2007) of the inlets was 60mm. The inlets were fitted to one or more sides of the codend in T45 configuration (meshes turned 45 degrees to achieve a square-mesh shape). Therefore, the reduced size and square shape (T45) of the inlet meshes render size selection of flatfish negligible, at least for the range of sizes available in the fishing grounds used. The first design tested during the sea trials was achieved by blinding the bottom and lateral sides of the FD40_110 codend. Thus, only the top-side of the codend was selective (FD40_110_top, Figure 6-1). The second design tested was achieved by moving the inlet from the bottom side of the previous design to the top side, thus, only the bottom panel of the codend was selective (FD40_110_bottom, Figure 6-2). The third codend design was achieved by blinding both the bottom and top sides of the codend, thus, only the lateral sides of the codend were selective (FD40_110_sides, Figure 6-3). Finally, the last design tested was achieved by removing all the inlets from the codend (FD40_110_full, Figure 6-3). This codend design is the same as tested during "Solea" cruise no 797, and therefore it should deliver the baseline selectivity.

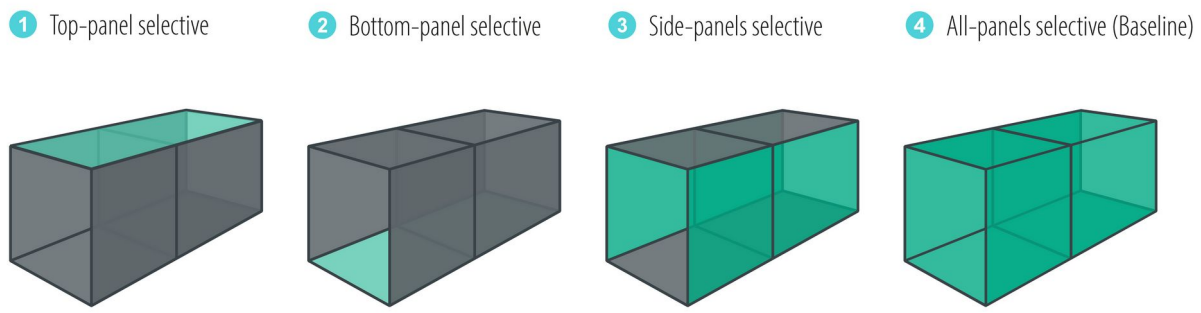

Figure 6: illustration of the four different codend designs tested during the trials. Each codend design was tested for one fishing day and the order of testing follows the sequence in the figure, from left to right. Codend panels in grey are those that were blinded by small-mesh netting and, therefore, are non-selective for the species considered in the study. Panels in green are those left uncovered, thus providing the available size selection of each design.

Data Collection and sampling procedures

Escapees resulting from the size selection of the experimental codends (*CD*) were collected using the cover codend method (Wileman *et al.*, 1996; Wienbeck *et al.*, 2011, 2014). The cover (*CC*) is made of single 2.5 mm-PE twine and a nominal mesh size of 55mm, it has a stretched length of ~16 m (2.6 x the length of the extension piece and rigid codend combined) and a diameter of ~3 m. In order to prevent the cover from masking the selectivity of the codend, a total of seven kites were attached to the cover to keep a stable and sufficient physical separation between both compartments. Five kites were attached to the forward section and the remaining two were attached two each side of the cover. The catches obtained at haul level were sampled for each compartment and fish species separately.

Figure 7: Lateral view of the experimental FD40_110 codend surrounded by the cover. The cover was rigged with forward (red, green and grey) and lateral kites aligned to the mid-length of the codend (grey). To compensate for the negative buoyancy of the FD40_110 codend, the device was initially rigged with 2x floating lines consisting of 7x foam buoys that were attached side by side along the longitudinal upper bars of the frame.

Catches obtained in the codend and the cover at haul level were sampled separately by species. When possible, all fish were measured. In case of excessive catches of a given species, a random sub-sample was obtained from the total, and the ratio of sub sampled weight to the species total catch weight was calculated as sampling factor.

Underwater Video Recording were collected haul by haul using UW cameras *insta360* . The availability of UW cameras with 360 view capabilities can dramatically increase the FOV delivered by standard UW cameras, facilitating the tracking of individual fish performing escape attempts. Therefore, the collection and analysis of selectivity -catch data, in conjunction with the potential behavioral information provided by the video recordings should produce new knowledge regarding escape behavior of flatfish in the codend.

The current report focuses on results obtained from the catch-data analysis. The video footage taken during the cruise will be processed and analyzed as part of a master's thesis due to start in September 2024.

Analysis of catch-data

Estimation of codend selectivity

The size selection delivered by each of the experimental codend was analyzed by species using the traditional methodology described in Wileman et al. (1996). Traditional codend selectivity analysis assumes that (a) the proportion of fish retained in the codend is determined by the ability of the

fish to pass through the codend meshes, and (b) that this ability depends on how well the morphology and size of the individual fish matches the geometry and size of the meshes. These basic assumptions allow modeling the codend retention probability *r(l)* by simple mathematical functions with parametric structures leading to non-decreasing, s-shaped selectivity curves (Figure 8) asymptotically restricted to values between [0, 1] (Millar and Fryer, 1999; Wileman et al., 1996). The most often applied selectivity functions are the logistic, *probit*, g*ompertz*, and *Richards:*

$$r(l,\mathbf{v}) = \begin{cases} logit = \frac{exp(\frac{ln(9)}{SR}\times(l-L50)}{1+exp(\frac{ln(9)}{SR}\times(l-L50)} \\ probit \approx \Phi\left(1.349 \times \frac{(l-L50)}{SR}\right) \\ gompertz \approx exp\left(-exp\left(1.573 \times \frac{(l-L50)}{SR} - 0.366\right)\right) \\ Richards = \left(\frac{exp\left(logit(0.5^{\delta}) + \left(\frac{logit(0.75^{\delta}) - logit(0.25^{\delta})}{SR}\right)\times(l-L50)\right)}{1.0+exp\left(logit(0.5^{\delta}) + \left(\frac{logit(0.75^{\delta}) - logit(0.25^{\delta})}{SR}\right)\times(l-L50)\right)}\right)^{\frac{1}{\delta}} \end{cases} \quad \text{(Eqs. 1)}$$

Where **v** is the vector of selectivity parameters that defines the selection curve. These include the L50 (fish length associated to 0.5 retention rates (50%)) and SR (range of lengths between lengths associated to 0.75 and 0.25 retention rates) Note that the Richards involves an additional parameter δ, which adds flexibility to the otherwise parametrically constrained functional forms delivered by the other three functions.

The expected number of fish retained and escaped from the codend can be directly related to the total number of fish entering the codend n_l and the selection curve (Eq. 1):

$$\begin{aligned} n_{l,cd} &= n_l \times r(l,\mathbf{v}) \\ n_{l,cc} &= n_l \times (1.0 - r(l,\mathbf{v}) \end{aligned} \quad \text{(Eq. 2)}$$

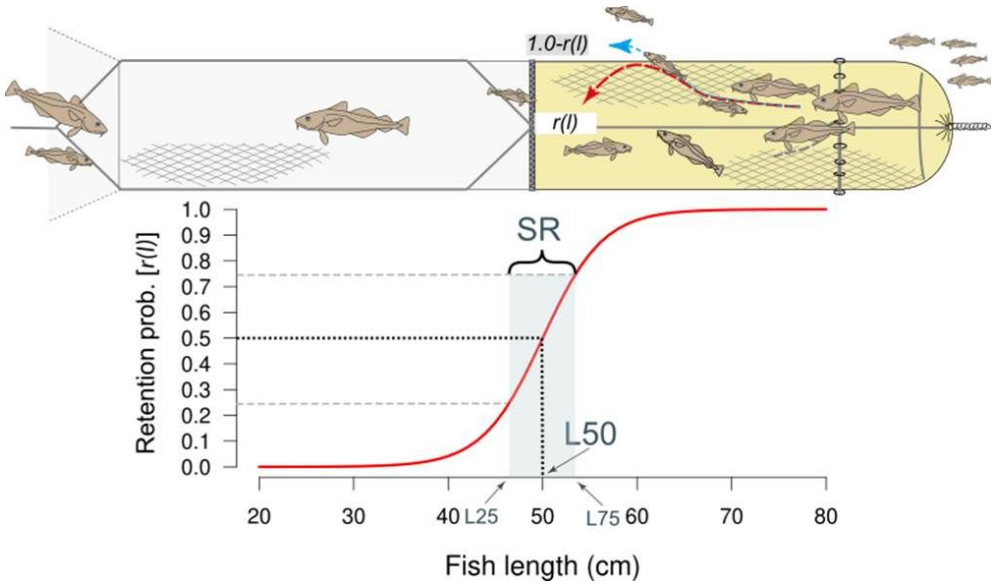

*Figure 8. Top: representation of a size-selection process in the codend. Bottom: example of a retention curve describing codend retention probability, with associated parameters L50 and SR. The notation referred to retention curve r(l) in the figure is an abbreviation of r(l,**v**) in text.*

In a size selection process, it can be hypothesized that a fraction of fish that enter the codend might not make an efficient contact with the mesh openings, and consequently those individuals will not be subjected to size selection. To cope with this situation, traditional size-selection models can be extended by introducing an additional parameter that accounts for the fraction of the fish that, having entered the codend, contacted the meshes becoming available for size selection. The sequence of these two probabilistic events defines the length-dependent contact retention (Millar and Fryer, 1999; Sistiaga et al., 2010):

$$r_c(l, \mathbf{v}) = C \times r(l, \mathbf{v}) \qquad \text{(Eq. 3)}$$

where the parameter *C* quantifies the fraction of the fish that contacted the mesh opening, and *r(l)* represents the available size selectivity in the codend described by any of the functions presented in Eqs. 1. Under the assumption that only a fraction of the fish entering the codend will make an effective attempt to escape through the codend meshes, the expected number of fish retained and escaped from the codend can be expressed as it follows:

$$n_{l,cd} = n_l \times (r_c(l) + (1.0 - C))$$
$$n_{l,cc} = n_l \times (1.0 - r_c(l)) \qquad \text{(Eq. 4)}$$

Another valid assumption to describe size selection of a codend is the co-existence of more than one average size selection signature. In the case of assuming a dual selection process, then it

should be expected that a fraction of fish entering the codend will be available to one of the size selection signatures, while the remaining fish will be selected by the other size selection signature. This process can be mathematically described by extending Eq. 3:

$$r_{s2}(l, \mathbf{w}) = C \times r_1(l, \mathbf{v}_1) + ((1.0 - C) \times r_2(l, \mathbf{v}_2)) \quad \text{(Eq. 5)}$$

Where $\boldsymbol{v_1}$ and $\boldsymbol{v_2}$ are the vector of selectivity parameters defining the two size selection processes considered, and $\boldsymbol{w = (v_1, v_2)}$.

The cover-codend experimental method applied in this study enables collecting the retained and escaped fish respectively in the codend (*CD*) and the cover (*CC*). The values of the selectivity parameters associated to Eqs. 1,3 and 5 that makes the catch data most likely were estimated via Maximum Likelihood. The procedure involves minimizing the negative of the log-likelihood of the following binomial probability mass function:

$$-\sum_i \sum_l (n_{il,cd} \times log(r(l)) + n_{il,cc} \times log(1.0 - r(l)) \quad \text{(Eq. 6)}$$

Eq. 6 introduces the summation over hauls $h \in \{i=1,...,m\}$, being $n_{il,cd}$ and $n_{il,cc}$ the fish sampled in haul *i*. Thus, assuming that the *m* hauls were randomly drawn from all possible hauls that could be conducted, Eq. 6 returns an estimate of the population-average selectivity properties of the codend tested. All models described in Eqs. 1,3 and 5 were estimated and ranked by AIC (Akaike, 1974), and the best candidate model was picked for further analysis.

To account for the variability between hauls of the size selection process (Fryer, 1991), and the uncertainty in model estimation, usually affected by the limited number of fish measured at haul level, a bootstrap technique was implemented based on the method proposed in Millar (1993). Thus, 95% confidence intervals of the average retention curves and associated parameters were approximated by the histogram based on the resulting bootstrap distributions using the percentile method (Efron, 1979)

Evaluation of differences in selectivity among the tested codends

The ultimate aim of the catch-data analysis is to assess differences in selectivity among the four tested codends. Thus, considering the estimated selectivity of the FD40_110_full codend as the baseline selectivity in the assessment, pairwise comparisons with the retention probability at length estimated for the remaining codend designs can be conducted as it follows:

$$\Delta r(l) = r_t(l) - r_0(l) \qquad \text{(Eq. 7)}$$

Eq. 7 quantify the absolute differences between the retention probabilities at length *l* estimated for the baseline codend design $\mathrm{r}_0(l)$ and any of the other tested designs, $\mathrm{r}_t(l)$. In order to test the null hypothesis $\mathrm{H}_0 : \Delta r(l) = 0.0$, the 95% percentile confidence intervals are estimated from a bootstrap distribution derived from the bootstrap distributions previously generated for $\mathrm{r}_b(l)$ and $\mathrm{r}_t(l)$:

$$\Delta r^{*b}(l) = r_t^{*b}(l) - r_0^{*b}(l) \qquad \text{(Eq. 8)}$$

Thus, significant differences would be found when the 95% confidence intervals *around* $\Delta r(l)$ *do not* overlap the value associated to the null hyphotesis $\mathrm{H}_0 : \Delta r(l) = 0.0$.

Evaluation of sources of uncertainty in the selection process

The bootstrap technique is further utilized in the analysis to isolate, evaluate and quantify sources of variation acting on the size selection process delivered by each of the codends tested. In particular, it is of interest to isolate and quantify the variability coming from the limited sampling size (often referred to as within-haul variation), and from the variation occurring between hauls (attributed to unaccounted and silent variables affecting the size selection at haul level).

3 Cruise narrative and preliminary results

3.1 Research Topic 1

The executed hauls were important to test the system. Unfortunately we experienced a series of technical issues, that resulted in imperfect images and connection to the system. We could solve some of the issues during the cruise, some where solved later and the system proved to be working well on Cruise SO832.

Figure 9: (upper row) Working on issues of the microcontroller, (lower row) Net with SmartFishing-System while deploying.

We could also determine that control over exposure time and light intensity is important to the image quality.

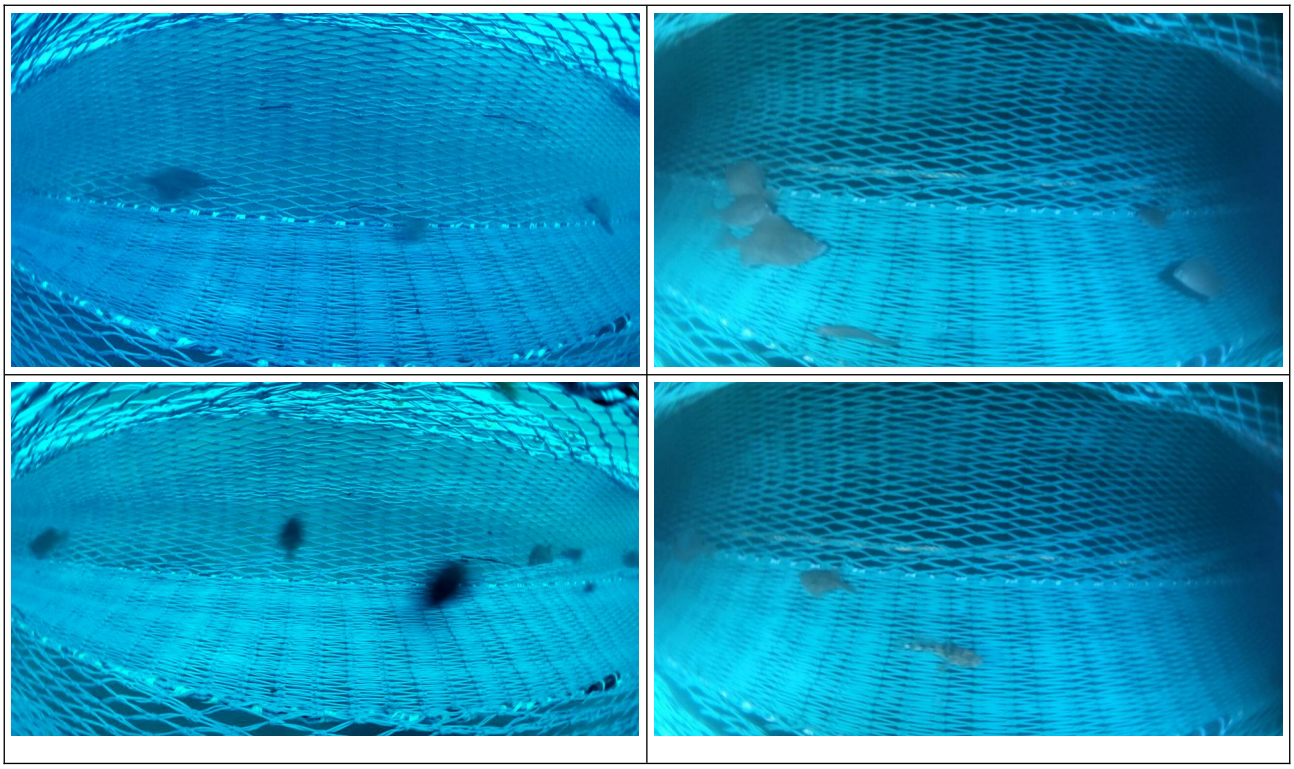

The images taken without artificial lighting suffered from blurring, due to misconfigured exposure-time. The issue couldn’t be solved during the cruise, but with the use of artificial light the problem could be reduced.

3.2 Research Topic 2

All codends were successfully tested during the four available fishing days without incident. The pre-defined experimental design was fully implemented, resulting in a total of 20 valid hauls (five per codend design, Table 1). Weather conditions and other environmental factors were stable over the four fishing days, as well as catches of relevant species. As expected, plaice and dab dominated the catch, while catches of other species such as flounder, turbot, cod and whiting were scarce. Further information related to fishing operations and catches can be found in Table 1. Selectivity data of the two most caught flatfish species, plaice and dab, is showed in Figures 10 and 11, respectively.

All models considered in Eq 1-5 were successfully fitted to the plaice data using the Maximum Likelihood method (Eq. 6). Of these, the outputs from the best candidate models (based on AIC), picked for further analysis are showed in Table 2. The average retention curves with 95% confidence intervals estimated for each codend are showed in Figure 12. The baseline codend (FD40_110_full) and the design with the lateral sides selective (FD40_110_sides) delivered very similar retention curves. In both cases de retention curves were sharp and positioned around the species MCRS (25 cm, Figure 12). The design with the top side selective (FD40_110_top) delivered a significantly lower L50 and a significantly higher SR than the two previous designs. Finally, the bottom-selective design (FD40_110_bottom) gave a poorly defined retention curve. The pairwise comparisons between the baseline codend and the remaining codend designs reveals significantly higher retention by the FD40_110_top and the FD40_110_bottom codends. In contrast, using the codend with only the sides selective does not lead to any difference in the retention probability relative to the baseline codend (Figure 13).

The results obtained for dab are consistent with those obtained for plaice, and the outputs from the best candidate models are showed in Table 3. The average retention curves with 95% confidence intervals estimated for dab and each codend are showed in Figure 14. Again, the baseline design (FD40_110_full) and the design with the lateral sides-selective (FD40_110_sides) delivered very similar retention curves, being the cLogistic the best candidate model for both designs (Table 3). The resulting retention curves show less sharp patterns than the retention curves estimates for plaice, but similarly positioned around dab length = 25 cm. Again, the top-selective design (FD40_110_top) gave a significantly lower L50 and a significantly higher SR than the two previous designs, while the bottom-selective design (FD40_110_bottom) delivered the poorest retention curve. The results of the pairwise comparisons of dab retention curves are also consistent with those obtained for plaice: it is found a significantly higher retention by the FD40_110_top and the FD40_110_bottom codends, while the FD40_110_sides codend delivers comparable retention probabilities to the baseline codend (Figure 15).

Table 1: Operational information of the hauls conducted during the cruise related to the research topics 1 and 2, and total number of individuals from relevant species caught by haul and length-measured (in brackets, the fraction of the measured fish that were observed in the codend).

Research Topic	test design	haul	time	latitude	longitude	depth	duration	COD	PLE	FLE	DAB
1	FWR_CAM_test	1	2023/10/27 10:59:59	54°11,9	11°59,4	16	15.13	12	262	1	368
	FWR_CAM_test	2	2023/10/27 12:08:54	54°12,2	12°00,0	15	12.08	7	260	2	56
	FWR_CAM_test	3	2023/10/27 13:27:29	54°12,2	11°59,5	16	15.07	2	92	NA	50
	FWR_CAM_test	4	2023/10/28 06:30:12	54°12,2	11°59,7	16	30.05	23	624	8	225
	FWR_CAM_test	6	2023/10/28 09:05:24	54°12,2	11°57,5	18	30.03	3	468	14	319
	FWR_CAM_test	7	2023/10/28 10:58:12	54°12,2	11°59,7	16	30.03	7	459	11	357
	FWR_CAM_test	8	2023/10/28 12:17:42	54°12,2	12°00,0	15	30.05	3	814	7	253
	FWR_CAM_test	9	2023/10/28 14:01:50	54°11,7	11°54,9	18	30.03	15	657	5	334
	FWR_CAM_test	10	2023/10/29 05:26:58	54°12,2	11°59,6	16	30.05	1	388	2	280
	FWR_CAM_test	11	2023/10/29 07:35:51	54°11,8	11°55,3	18	30.03	6	316	4	129
2	FD40_110_top	12	2023/10/30 06:41:05	54°12,0	12°00,1	15	30.05	13(1)	920(605)	5(5)	245(145)
	FD40_110_top	13	2023/10/30 07:37:33	54°11,9	11°56,2	18	30.03	7(1)	946(484)	9(8)	511(281)
	FD40_110_top	14	2023/10/30 09:04:24	54°12,2	11°59,6	16	30.07	5(0)	587(349)	5(2)	516(276)
	FD40_110_top	15	2023/10/30 11:10:00	54°12,1	11°59,8	15	30.05	7(7)	795(381)	6(6)	459(304)
	FD40_110_top	16	2023/10/30 12:39:43	54°11,7	11°56,1	17	30.03	5(4)	785(322)	9(8)	395(134)
	FD40_110_bottom	17	2023/10/31 07:17:49	54°11,9	11°58,9	16	30.03	1(1)	485(444)	5(3)	209(177)
	FD40_110_bottom	18	2023/10/31 08:14:06	54°11,7	11°55,3	18	30.05	13(8)	1024(932)	13(13)	424(349)
	FD40_110_bottom	19	2023/10/31 09:02:31	54°12,2	11°58,1	17	30.03	1(1)	160(154)	4(4)	131(128)
	FD40_110_bottom	20	2023/10/31 10:14:33	54°12,2	11°56,8	18	30.05	9(2)	466(416)	NA	148(102)
	FD40_110_bottom	21	2023/10/31 11:08:08	54°12,2	11°59,8	16	30.03	6(3)	190(169)	2(2)	387(330)
	FD40_110_sides	22	2023/11/01 06:40:33	54°12,0	11°59,9	16	30.03	20(1)	842(158)	6(6)	195(27)
	FD40_110_sides	23	2023/11/01 07:37:00	54°12,0	11°56,5	18	30.07	16(3)	533(64)	11(10)	468(54)
	FD40_110_sides	24	2023/11/01 08:59:46	54°11,3	11°53,9	19	30.05	11(1)	590(106)	3(3)	400(59)
	FD40_110_sides	25	2023/11/01 11:07:50	54°12,0	11°59,6	16	30.05	17(3)	298(80)	6(5)	220(20)
	FD40_110_sides	26	2023/11/01 12:40:33	54°11,7	11°55,8	18	30.05	7(1)	571(93)	7(3)	382(39)
	FD40_110_full	27	2023/11/02 06:42:58	54°11,9	11°58,8	16	30.05	4(2)	342(88)	13(11)	199(34)
	FD40_110_full	28	2023/11/02 07:41:27	54°11,5	11°54,9	19	30.05	1(1)	489(58)	3(2)	396(44)
	FD40_110_full	29	2023/11/02 09:01:04	54°12,2	11°58,0	17	30.03	7(1)	349(57)	6(4)	210(30)
	FD40_110_full	30	2023/11/02 09:53:47	54°11,5	11°54,9	19	30.02	9(2)	404(78)	6(1)	421(61)
	FD40_110_full	31	2023/11/02 11:43:12	54°12,2	11°59,0	16	30.03	NA	301(77)	9(5)	336(40)

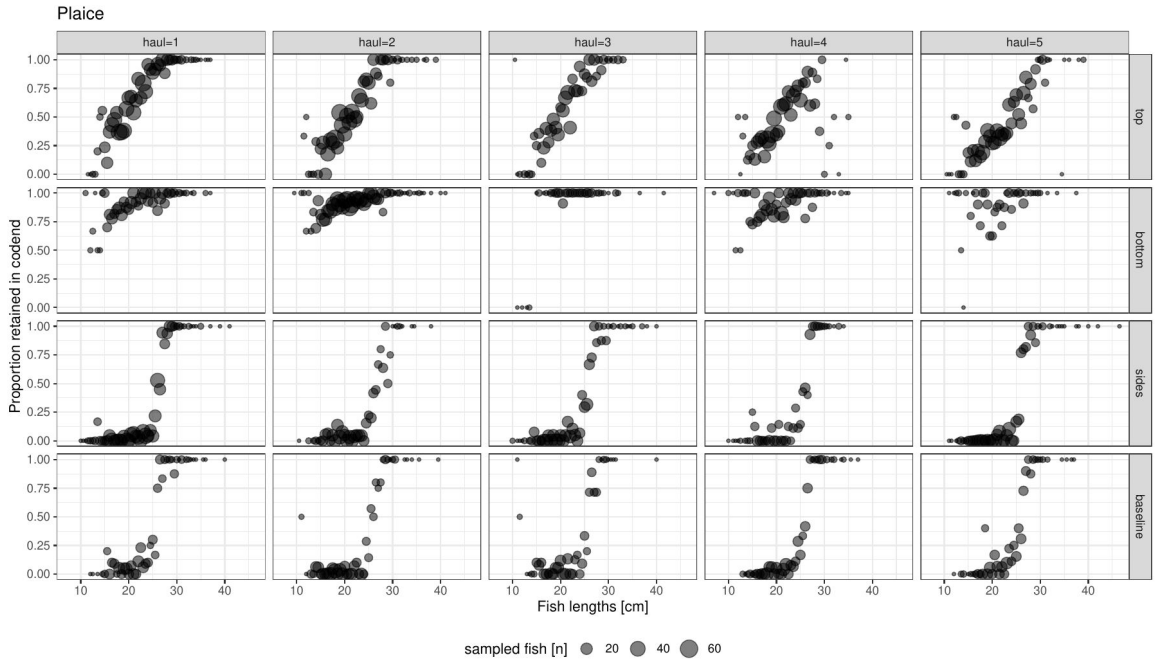

*Figure 10: Proportion of total **plaice** caught per haul retained in the codend. Rounded marks: experimental retention rates at length. The information is presented separately for each codend design by rows (top = top panel selective (FD40_110_top), bottom=bottom side selective (FD40_110_bottom), sides=lateral sides selective (FD40_110_sides) baseline=all four sides selective (FD40_110_full).*

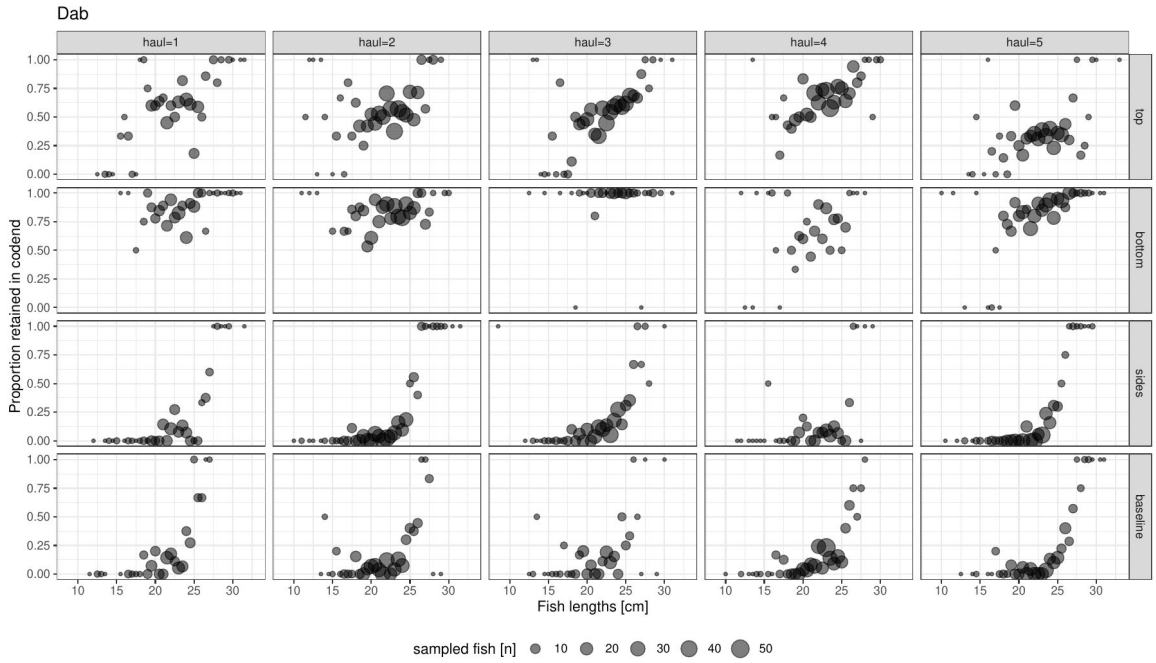

*Figure 11: Proportion of total **dab** caught per haul retained in the codend. Rounded marks: experimental retention rates at length. The information is presented separately for each codend design by rows (top = top panel selective (FD40_110_top), bottom=bottom side selective (FD40_110_bottom), sides=lateral sides selective (FD40_110_sides) baseline=all four sides selective (FD40_110_full).*

Table 2: Best candidate models for plaice data and the four different test codends

test codend	model	L50(c)	SR(c)	D	C	L501	SR1	loglik	nbetas	aicc
FD40_110_top	cLogistic	21.31	7.70	NA	0.93	NA	NA	111.48	3.00	229.44
FD40_110_bottom	Probit	4.47	15.94	NA	NA	NA	NA	74.77	2.00	153.75
FD40_110_sides	dLogistic	26.01	1.12	NA	0.86	26.34	9.54	66.90	5.00	144.94
FD40_110_full	cLogistic	25.84	1.61	NA	0.97	NA	NA	63.18	3.00	132.84

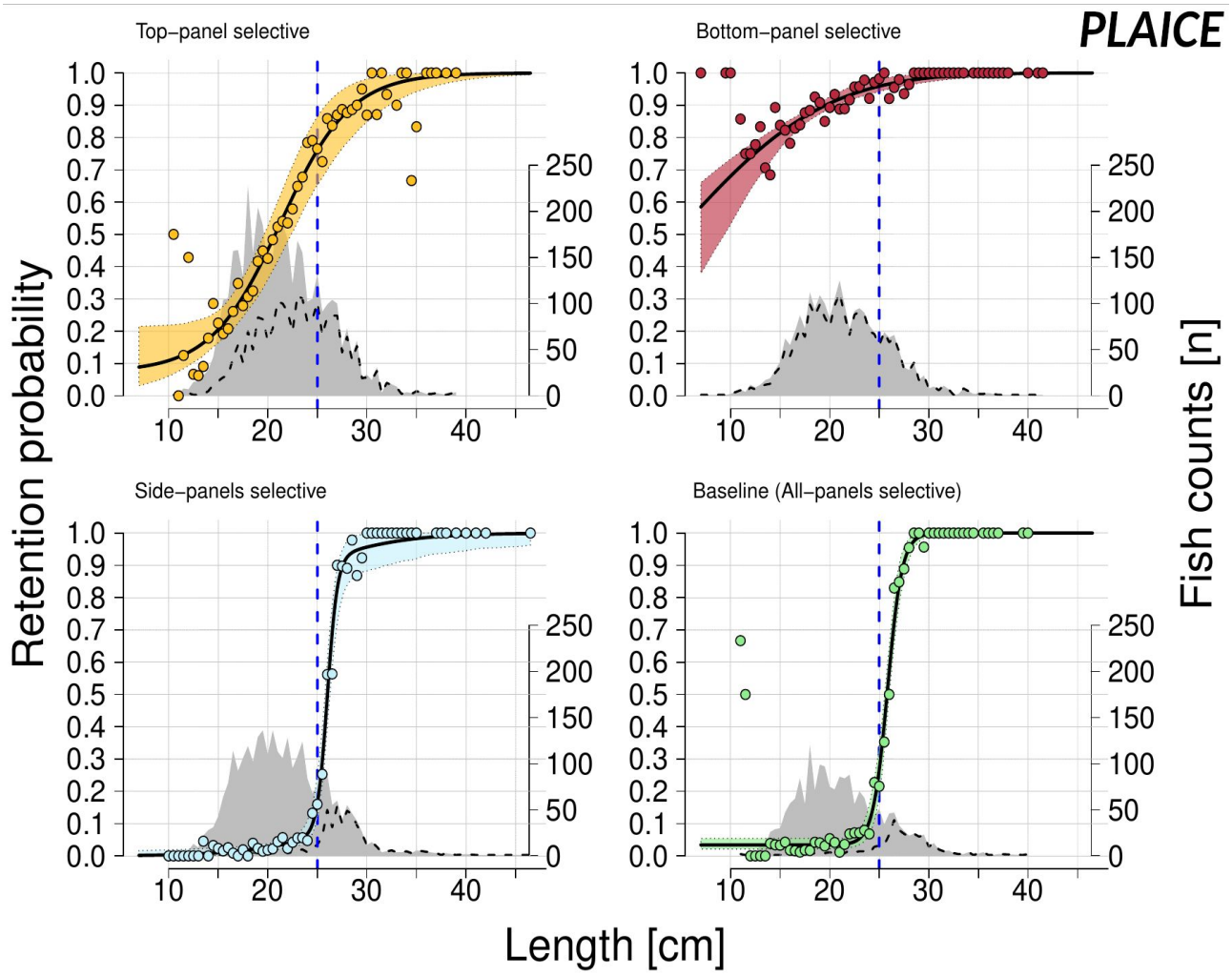

*Figure 12: Average selection curves estimated for **plaice** and for all tested codend designs. Color shaded areas: Confidence intervals of the selection curve. Rounded marks: experimental retention rates at length. Vertical dashed line: species MCRS (25 cm). Total catches represented at the bottom of the plots by a black dashed line (codend) and a dark grey polygon (codend + cover)*

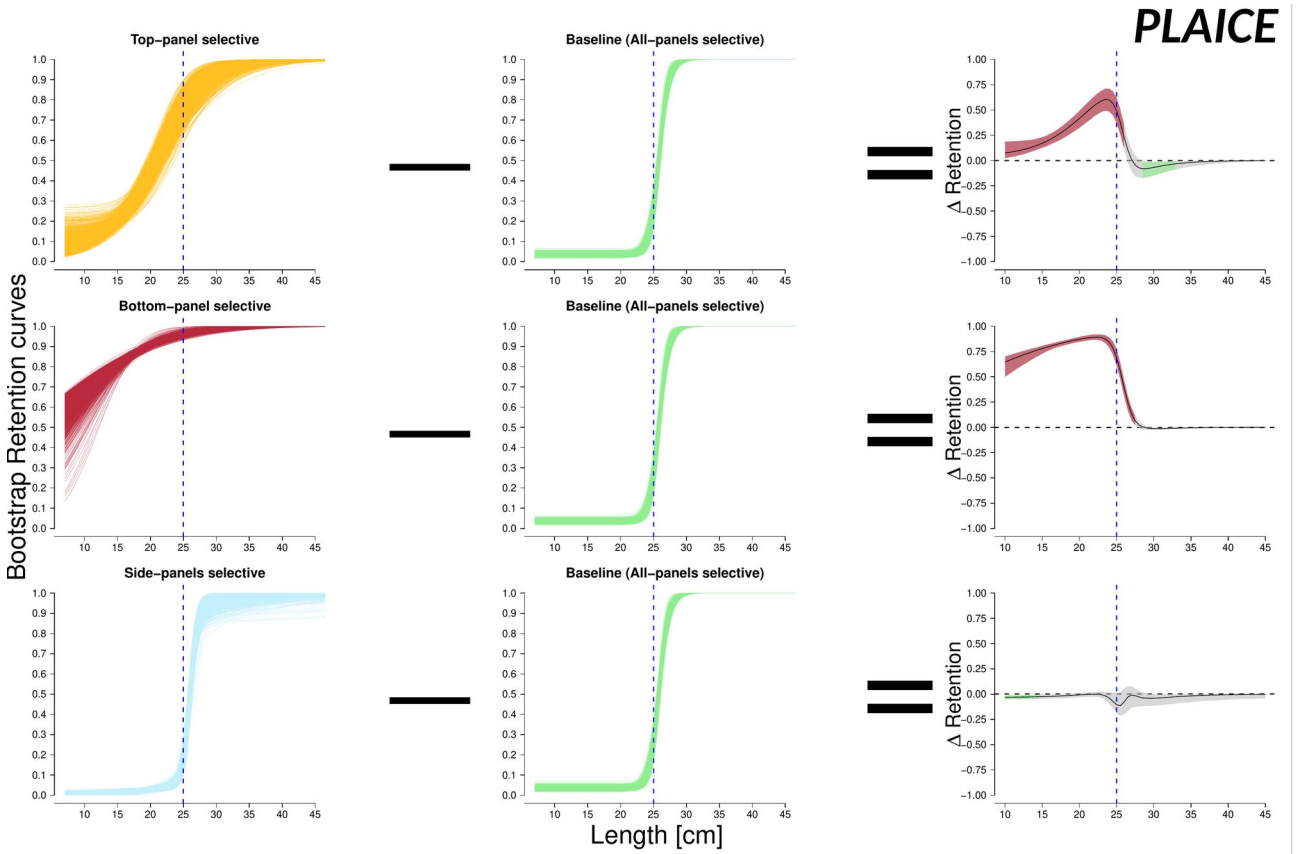

*Figure 13: Evaluation of the effect of spatial positioning and orientation of selective meshes on the size selection of **plaice**. Plots in the first and and second columns show respectively the bootstrap distributions of the selection curves obtained from the test codend designs and the baseline design (all codend panels selective). Plots in the third column show the average differences in selectivity (delta Retention), and associated confidence intervals. Horizontal line at delta Retention = 0.0 marks the null hypothesis of no differences in size selection between the tested and baseline modification. Significant higher and lower delta Retention represented by respectively red and green areas of the confidence intervals. Vertical dashed line: MCRS of plaice (25 cm).*

Table 3: Best candidate models for dab data and the four different test codends.

model test	model	L50(c)	SR(c)	D	C	L501	SR1	loglik	nbetas	aicc
FD40_110_top	dLogistic	16.65	18.41	NA	0.78	26.47	1.00	80.80	5.00	173.3143
FD40_110_bottom	Richards	4.27	39.64	534.98	NA	NA	NA	63.12	3.00	132.8634
FD40_110_sides	cLogistic	25.97	2.24	NA	0.97	NA	NA	54.37	3.00	115.3302
FD40_110_full	cLogistic	26.37	2.50	NA	0.95	NA	NA	56.44	3.00	119.5245

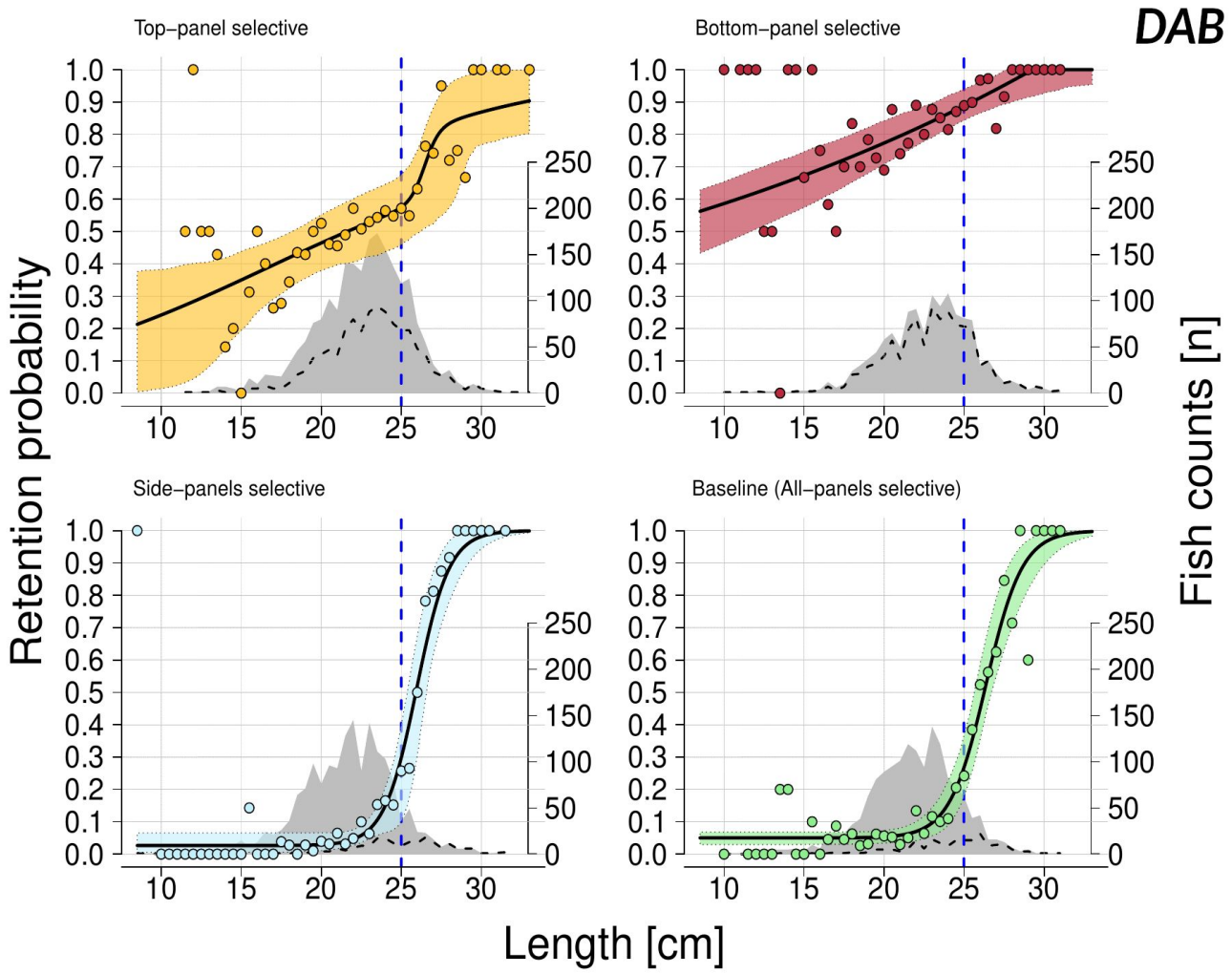

*Figure 14: Average selection curves estimated for **dab** and for all tested codend designs. Color shaded areas: confidence intervals of the selection curve. Rounded marks: experimental retention rates at length. Vertical dashed line: MCRS of plaice (25 cm) taken as references also for dab. Total catches represented at the bottom of the plots by a black dashed line (codend) and a dark grey polygon (codend + cover).*

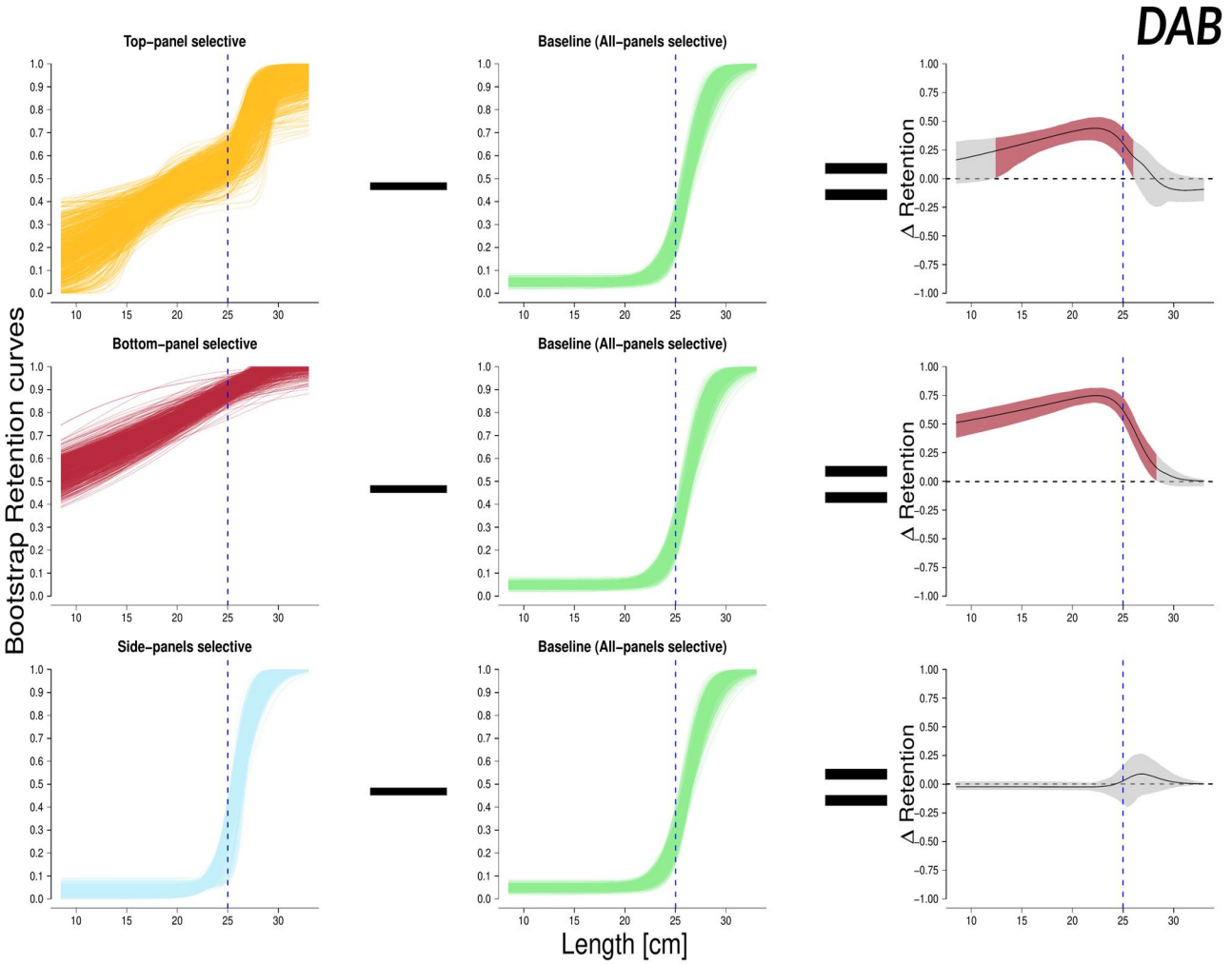

*Figure 15: Evaluation of the effect of spatial positioning and orientation of selective meshes on the size selection of **dab**. Plots in the first and and second columns show respectively the bootstrap distributions of the selection curves obtained from the test codend designs and the baseline design (all codend panels selective). Plots in the third column show the average differences in selectivity (delta Retention), and associated confidence intervals. Horizontal line at delta Retention = 0.0 marks the null hypothesis of no differences in size selection between the tested and baseline modification. Significant higher and lower delta Retention represented by respectively red and green areas of the confidence intervals. Vertical dashed line: MCRS of plaice (25 cm) taken as references also for dab.*

Evaluation of sources of uncertainty in the selection process

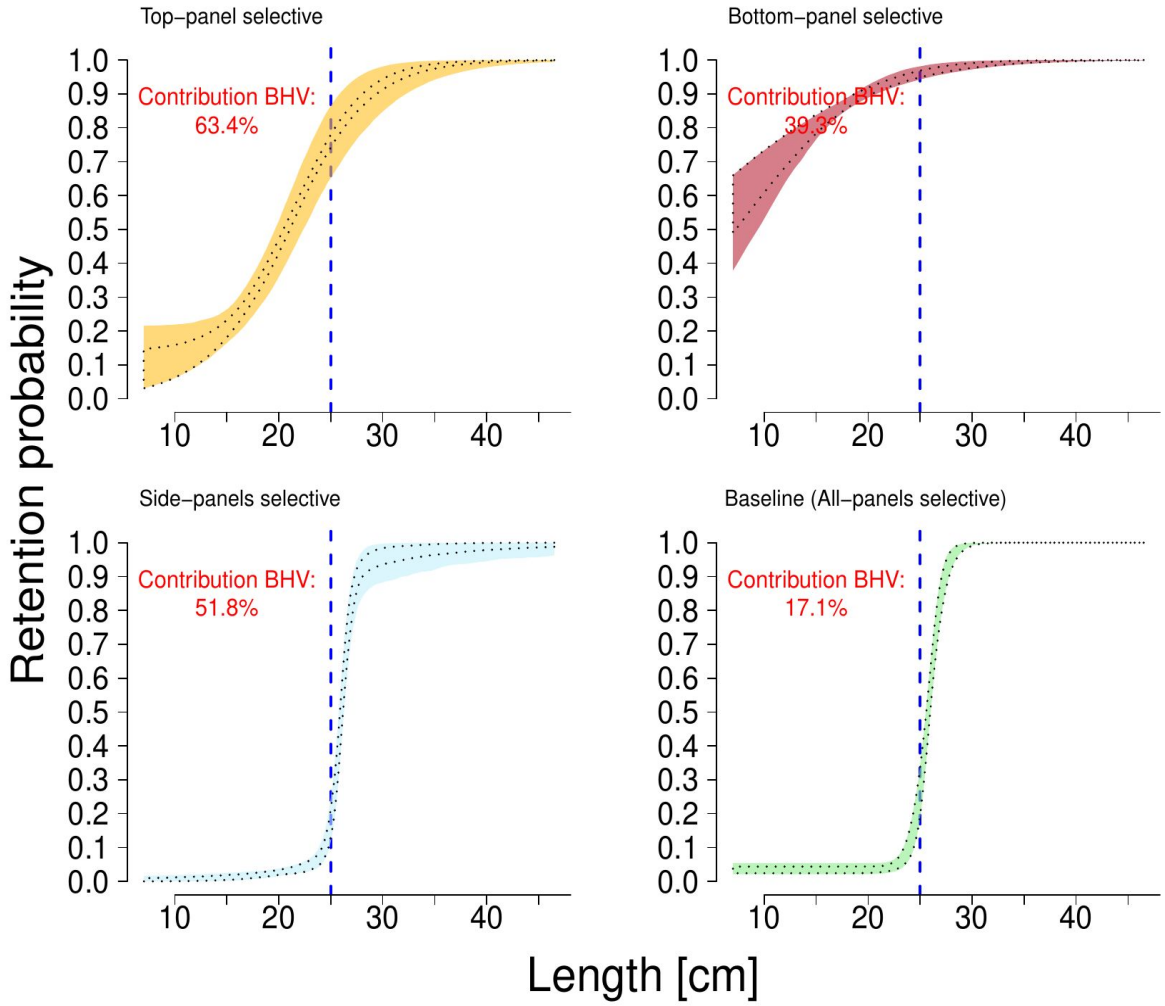

*Figure 16: Confidence intervals associated to the average retention curves estimated for **plaice** and the four codend designs tested. Coloured bands represent the confidence intervals estimated from the bootstrap distribution generated using the dual resampling scheme (haul replicates and fish samples within hauls). Dotted bands represent the confidence intervals estimated when only the inner resampling procedure (fish sampling) is considered. Contribution of between-haul variation, calculated as the ratio of the root mean square obtained from both resampling scenarios. The interpretation of these results have to be taken with caution due to the different model used and other aspects related to sources of uncertainties.*

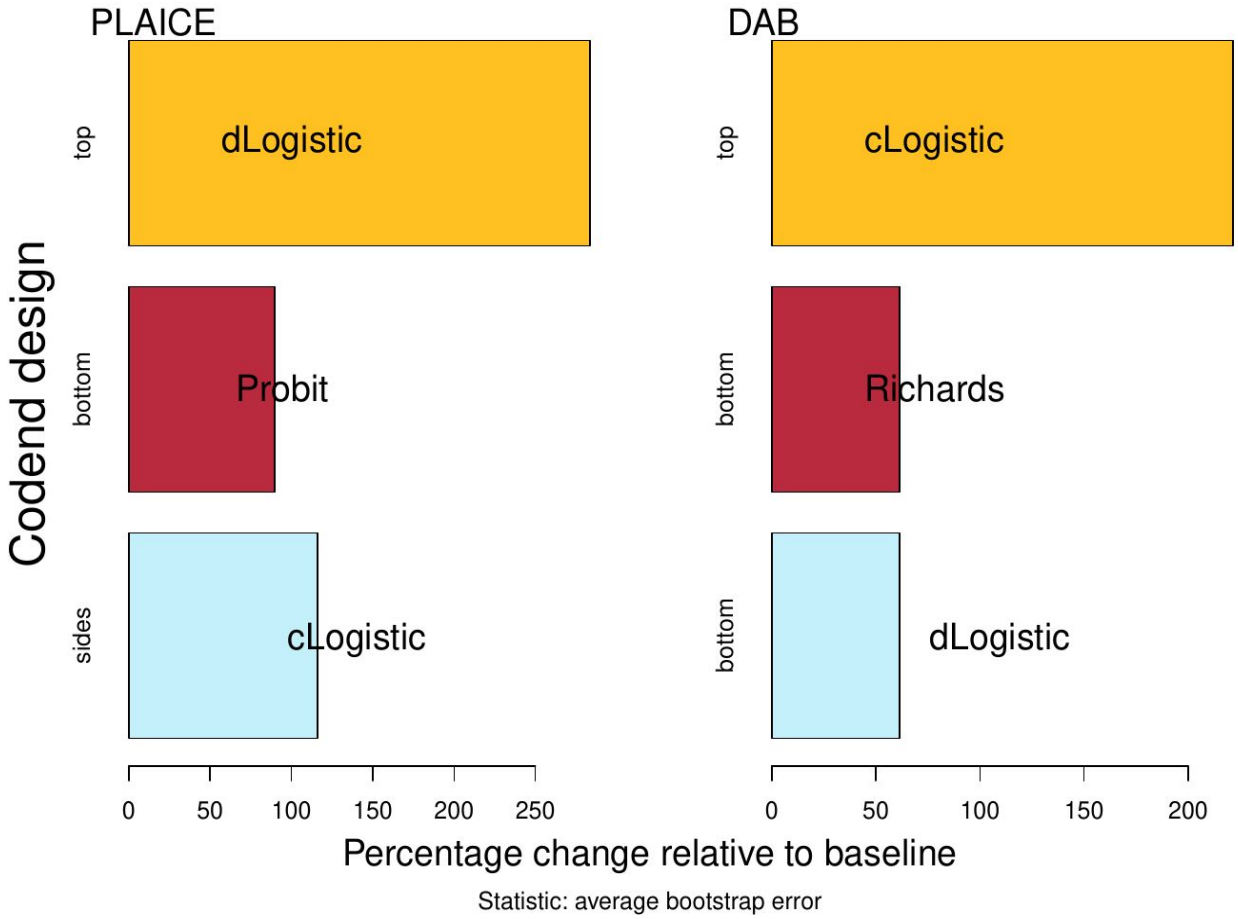

Figure 17: Overall estimated contribution of between-haul variation to the uncertainties in the estimation of the retention curves associated to the top-selective, bottom-selective and (lateral) sides-selective codend designs relative to the baseline design. The interpretation of these results have to be taken with caution due to the different model used and other aspects related to sources of uncertainties.

4 Final remarks

4.1 Research Topic 1

The results we got on this cruise are very important for the future development of the camera. While we didn't get optimal images, we still learned a lot about the handling of the camera and what to avoid in the future. Our experiments brought up several problems, that could be fixed in the time following the cruise, resulting in an excellent result in a repeated experiment in February 2024.

4.2 Research Topic 2

The results obtained show no significant differences in selectivity between the baseline codend design and the (lateral) side-selective design, despite the latter design having 50% fewer open meshes than the baseline for fish to escape. In contrast, clear and significant differences were found for the remaining designs. This supports the hypothesis that the use of an optimal escape option available in the codend (for flatfish, the wider axis of the diamond mesh opening) is more frequently used when attempting to make the required optimal contact with the meshes is energetically efficient, for example when it requires simple body turns and limited hydrodynamic disturbance. Assuming this is true, the meshes in the lateral sides of the codend were a priory identified as the most energy efficient escape option for flatfish. The results obtained therefore confirm our expectations.

For the top-selective and the bottom-selective codends, only 25% of the meshes were selective compared to the baseline codend. The selective meshes of the two designs had exactly the same orientation, and therefore it would require exactly the same body turns from the fish in order to use the escape possibility optimally. Therefore, the clear differences found between the retention curves and associated parameters obtained for each of these designs can only be explained by a preference to perform positive pitch turns rather than negative ones. -It would be interesting to build a general empirical model using all data collected for each species, adding covariates others than individual length as fixed effects, and the ratio of open meshes available for selection as offset.

-The very narrow confidence intervals obtained for the most efficient codend designs suggest that the limited number of hauls (5 hauls per design) conducted under very stable fishing conditions and catches were sufficient to carry out this investigation successfully.

- Besides the catch data, underwater video recordings from 3D and 2D cameras were successfully collected for most of the hauls. An ethogram based on visualizations of the video recordings was defined. Future analysis of the video footage will be essential to help interpret the results of analysing the catch data, and to better flatfish behavior in codend size selection

5 Cruise participants

Name	Time onboard	Affiliation	Position
Eke, Theresia	Full cruise	Uni Rostock	HiWi
Degner, Georg	RT1	FW Robotics GmbH	Mechanic Engineer
Mahler, Mathis	RT1	TI/OF	Engineer
Santos, Juan	Full cruise	TI/OF	Cruise leader
Schael, Peter	Full cruise	TI/OF	Technician
Schöps, Kerstin	Full cruise	TI/OF	Technician
Schulz, Mathias	RT1	FW Robotics GmbH	Electric Engineer
Annika Brüger	RT2	TI/OF	Scientist

6 Acknowlegments

Thanks to the crew of the FFS “Solea” for their hard work and willingness to complete the challenging program of the cruise in the very short time available. Their active participation and good decisions made were fundamental to the final success achieved. We are also grateful for the support of our colleagues on shore. Thanks go to Annemarie Schütz, who produced several of the drawings in the report. Special thanks to our colleagues from DTU-Aqua Bent Herrmann, Valentina Melli, and Zita Bak-Jensen, essential actors in RT2 who could not join the cruise due to constrictions in time and vessel room availability.

7 Bibliography

Akaike, H. 1974. A new look at the statistical model identification. IEEE Transactions on Automatic Control, 19: 716–723.

Efron, B. 1979. Bootstrap methods: another look at the jackknife. The Annals of Statistics, 7: 1–26.

Fonteyne, R., Buglioni, G., Leonori, I., and O’Neill, F. G. 2007. Review of mesh measurement methodologies. Fisheries Research, 85: 279–284.

Fryer, R. J. 1991. A model of between haul variation in selectivity. ICES Journal of Marine Science, 48: 281–290.

Millar, R. B. 1993. Incorporation of between-haul variation using bootstrapping and nonparametric estimation of selection curves. Fisheries Bulletin, 91: 564–572.

Wienbeck, H., Herrmann, B., Moderhak, W., and Stepputtis, D. 2011. Effect of netting direction and number of meshes around on size selection in the codend for Baltic cod (Gadus morhua). Fisheries Research, 109: 80–88. https://linkinghub.elsevier.com/retrieve/pii/S0165783611000385 (Accessed 6 May 2021).

Wienbeck, H., Herrmann, B., Feekings, J. P., Stepputtis, D., and Moderhak, W. 2014. A comparative analysis of legislated and modified Baltic Sea trawl codends for simultaneously improving the size selection of cod (Gadus morhua) and plaice (Pleuronectes platessa). Fisheries

Research, 150: 28–37. https://linkinghub.elsevier.com/retrieve/pii/S0165783613002348 (Accessed 6 May 2021).

Wileman, D. A., Ferro, R. S. T., Fonteyne, R., and Millar, R. B. 1996. Manual of methods of measuring the selectivity of towed fishing gears. ICES Cooperative Research Report, 215. International Council for the Exploration of the Sea (ICES), Copenhagen, Denmark.

ANNEX I

Technical drawings of the fishing trawls and devices

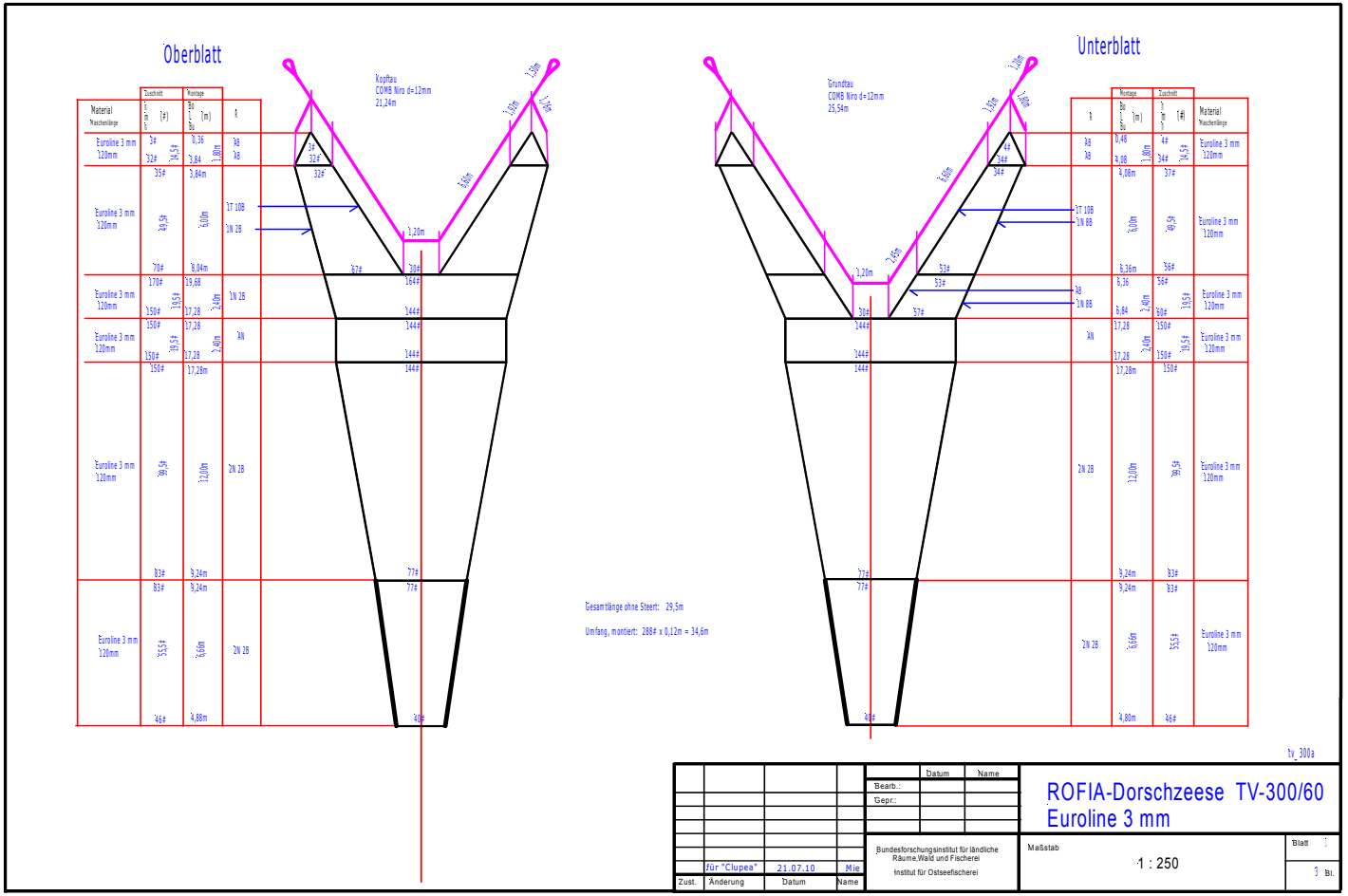

Figure A1- Technical drawing of the TV300/60 trawl.

Decksteert 16 m lang, 3 m Durchmesser, 200 Ansetzmaschen zum Teststeert

Zuschnittplan

PE geflochten; d= 2,5 mm; FM= 60 mm

4 Knoten in die Lasche (Zugabe ist in Maschenangaben enthalten)

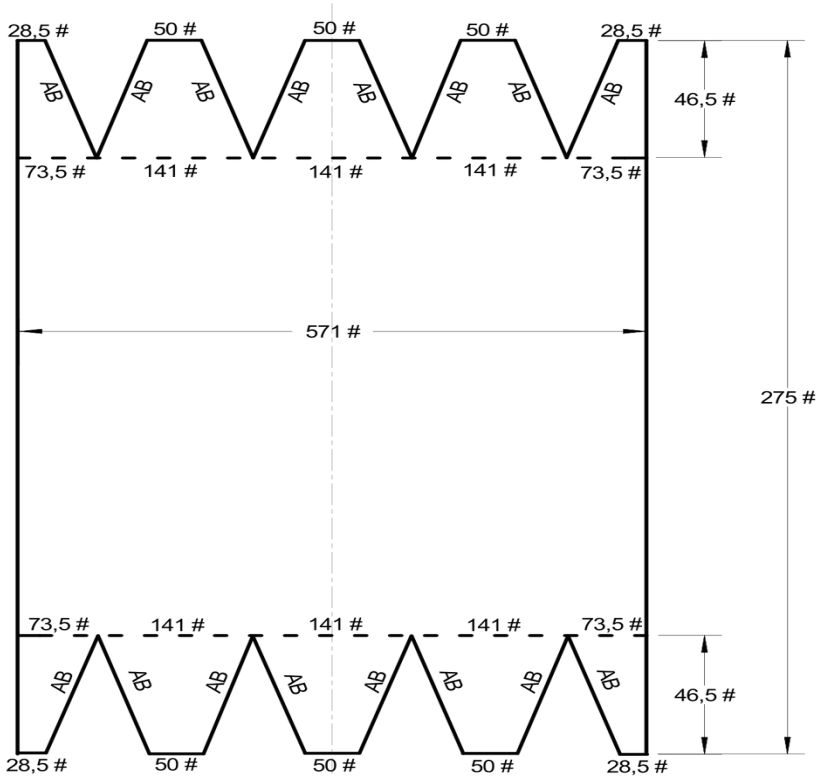

Blatt 1

Figure A2: Technical details of the cover codend used in RT2 .

ID	T0PE50S3_200#	Serial number	128

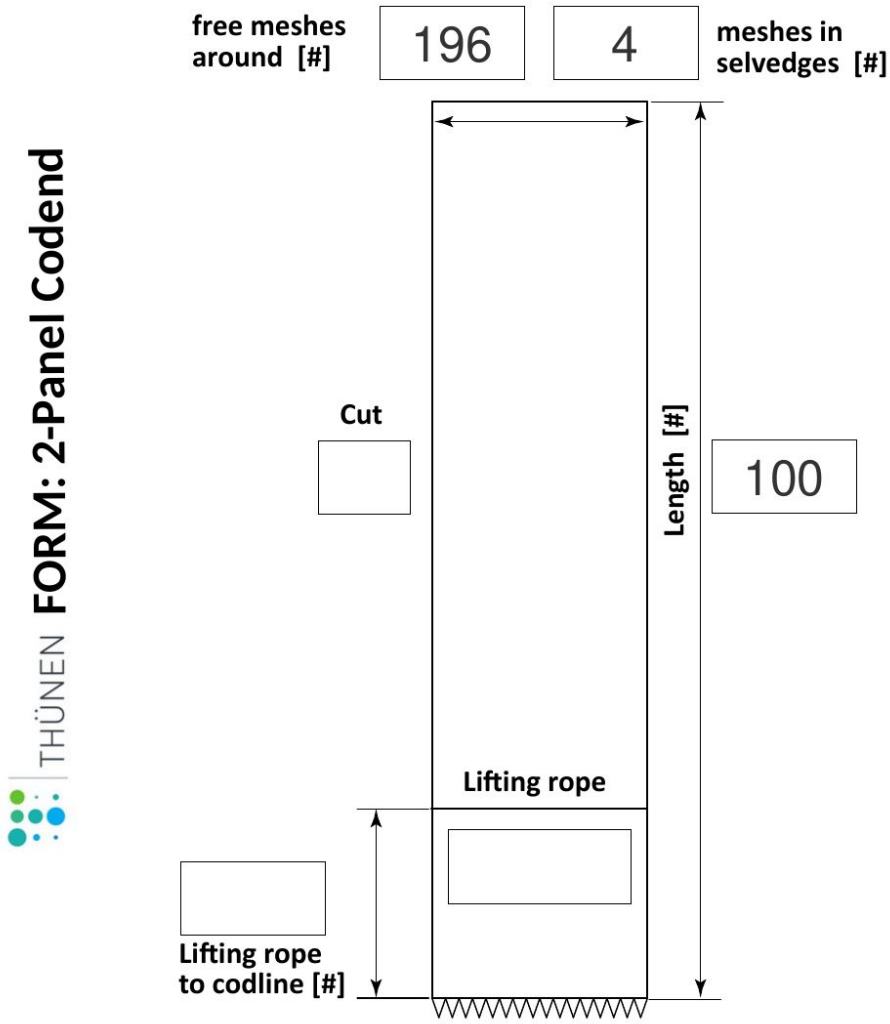

Netting and usage information	
Manufacturer /Year purchase	
Twine material / Weave/Color	PE/Braided/Green
Trade name	
Twine thickness [mm]	3
Twine in mesh [Single/Double]	Single
Nominal / Measured mesh size* [mm]	50/54.0
Measuring force [N]	125
Mesh orientation [°]	T0
Usage (Vessel + Cruise number)	SO696 ?
Additional information	Blind codend #2

*inner mesh size, measured according to Fonteyne (2007)

Figure A2: Technical drawing of the codend used in RT1.